THE JOURNAL OF PHYSICAL CHEMISTRY C
A JOURNAL OF THE AMERICAN CHEMICAL SOCIETY

pubs.acs.org/JPCC

Article

Twist-Induced New Phonon Scattering Pathways in Bilayer Graphene Probed by Helicity-Resolved Raman Spectroscopy

Bo Xu,[‖] He Hao,[‖] Jianqi Huang, Yan Zhao, Teng Yang, Jin Zhang, and Lianming Tong*

Cite This: *J. Phys. Chem. C* 2022, 126, 10487−10493

Read Online

ACCESS | Metrics & More | Article Recommendations | Supporting Information

ABSTRACT: The electron density of state near saddle points in an electronic band structure is greatly enhanced, forming the well-known Van Hove singularity (VHS), which leads to strengthened electron−photon coupling. However, the VHS-related electron−phonon interaction is rarely studied. Here we report the first observation of intra-mini valley phonon scattering pathways near the saddle points in twisted bilayer graphene (tBLG) through helicity-resolved Raman spectroscopy. Two new second-order Raman modes near the G peak are observed and assigned to combination modes of in-plane optical (TO, LO) and out-of-plane acoustic (ZA) mode, at ∼1580 cm^{-1} (TOZA) and ∼1595 cm^{-1} (LOZA), respectively. The twist-angle-dependence of their intensities and frequencies can be explained by double resonance Raman processes considering the fine electronic band structure of saddle points. Our findings provide a deeper understanding of the electronic band structure at saddle points of tBLG and enrich the VHS-related physics from an electron−phonon interaction point of view.

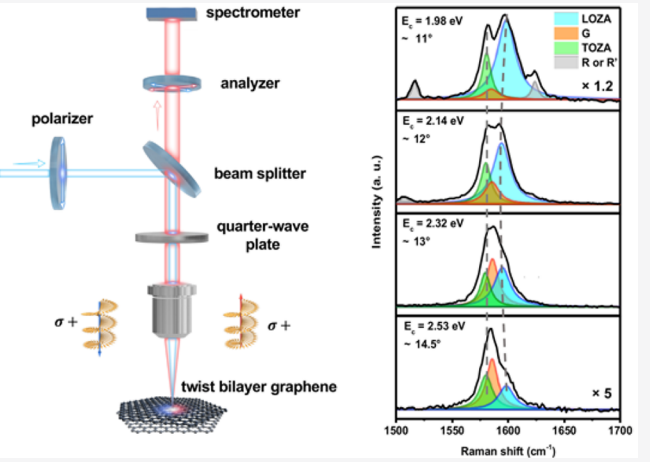

INTRODUCTION

The Van Hove singularity (VHS) is a divergence in the density of state (DOS), which can be generated at saddle points in electronic band structures.[1] Because of a large DOS at the VHS, electron−photon coupling will be greatly enhanced if the states are located at the VHS, which is the so-called VHS resonance effect.[2−6] Twisted bilayer graphene (tBLG), the stacking of two monolayer graphene with a twist angle θ, is an ideal platform to study VHS-related physics.[7,8] At a large twist angle ($\theta > 10°$), the linear dispersion is maintained near Dirac points of tBLG, but new low-energy saddle points (different from high-energy saddle points in single layer graphene[9−11]) are generated at the crossing points of Dirac cones coming from two adjacent layers. By tuning twist angles, the energy separation between two low-energy VHS can be modulated to fit the photon energy, which leads to the observation of optical absorption peak[2,3] and Raman intensity enhancement.[4−6]

Except for the widely studied low-energy saddle points, a mini band gap and two corresponding mini valleys are simultaneously created at the crossing point of overlapped Dirac cones from two graphene layers.[12,13] Theoretically, these mini valleys can also mediate electron−phonon scattering, in which the phonon wavevector $\mathbf{q}$ is much smaller than normal inter- or intravalley scattering in Dirac cones.[14] As these mini valley scatterings depend on the band structure near the VHS, studies of the related Raman process can provide detailed information about the fine band structure around the low-energy saddle points and deepen the understanding of VHS-related phenomena. However, these intra-mini valley scattering-related phonon modes have not been observed yet.

In this work, we report the first observation of Raman modes directly coming from intra-mini valley phonon scattering near the low-energy saddle points of tBLG. These two Raman active modes are overlapped with the G band in a nonpolarized configuration but can be revealed by helicity-resolved Raman spectroscopy (HRRS). The Raman mode at ∼1580 cm^{-1}, referred to as TOZA mode in this paper, is assigned to the combination mode of in-plane transverse optical (TO) and out-of-plane acoustic (ZA) modes. And the other at ∼1595 cm^{-1}, referred to herein as the LOZA mode, is assigned to the combination mode of in-plane longitudinal optical (LO) and ZA mode. The two modes can only be observed under the $\sigma+\sigma+$ configuration of HRRS, that is, by selecting the same helicity ($\sigma+$) of Raman scattered light as that of the excitation

Received: May 14, 2022
Revised: May 29, 2022
Published: June 15, 2022

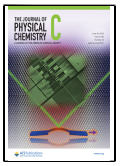

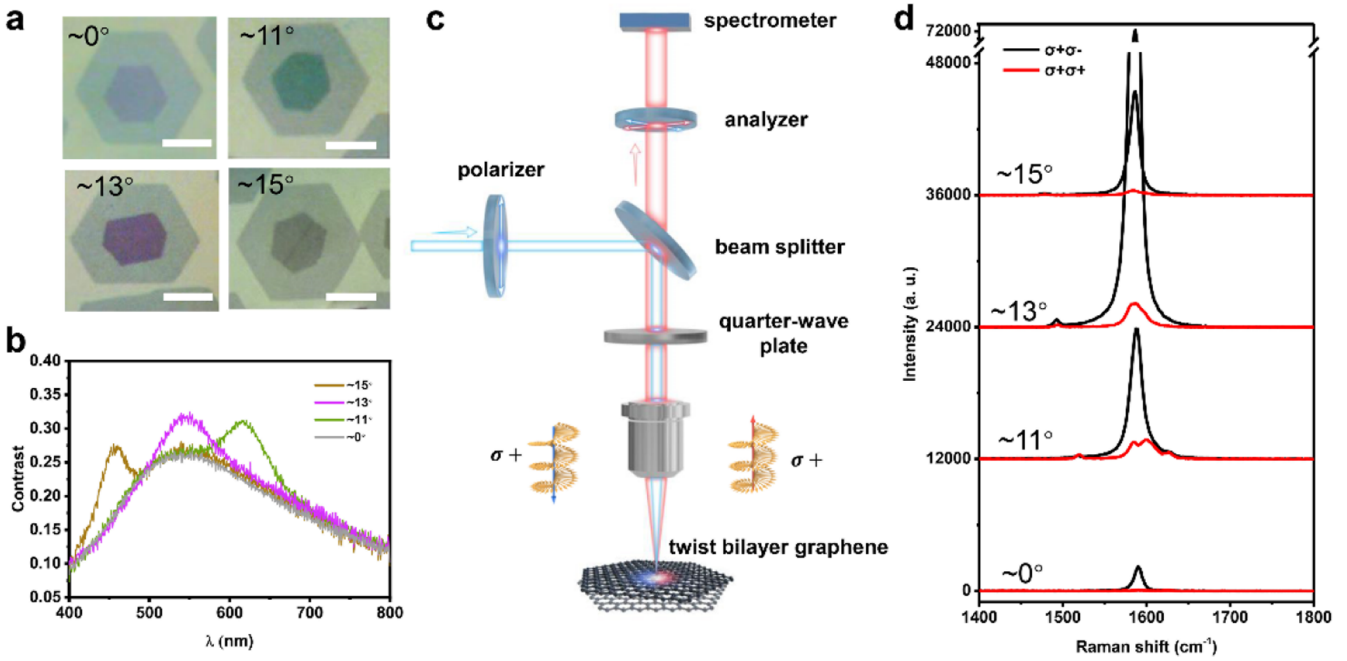

Figure 1. (a) Optical microscopy images of tBLG with a twist angle of ∼0° (Bernal-stacked BLG), 11°, 13°, and 15°. Scale bar, 5 μm. (b) Optical contrast spectra of tBLG in (a). (c) Schematic diagram for experimental setup of HRRS. (d) HRRS of tBLG in (a) under (σ+σ−) and (σ+σ+) configurations with 532 nm excitation. The critical angle is ∼13°.

laser (σ+), under which the intensity of the G mode is greatly suppressed due to Raman helicity selection rules. These two modes present the same VHS resonance behavior as that of the G mode, indicating that they share a similar resonance enhancement mechanism. Besides, the measured LOZA frequency is found to shift with the twist angle and excitation wavelength, while the frequency of TOZA remains almost unchanged. Together with our theoretical analysis, we verified that the phonon scattering pathways of LOZA and TOZA are near saddle points in the folded Brillouin zone, which indicates that these two phonon modes indeed arise from intra-mini valley scattering. Our results provide a wealth of information on the electronic band structure near low-energy saddle points in twisted bilayer graphene and enrich the VHS-related physics from the aspect of electron−phonon interaction.

METHODS

tBLG Sample Preparation. High-quality tBLG samples were grown via a chemical vapor deposition (CVD) method and transferred onto a SiO_2/Si substrate with the assistance of poly(methyl methacrylate) (PMMA). During the CVD process, a gas-flow perturbation and a heterosite nucleation strategy was employed to increase the fraction of tBLGs in bilayer graphene domains.[15] A piece of Cu foil (50 μm thick, Kunshan Luzhifa Electron Technology Co., Ltd.) was placed in a homemade CVD system that is equipped with a 3 in. quartz tube and sequentially heated to 800 °C (400 sccm Ar, 30 min), annealed (400 sccm Ar, 10 min), heated to 1020 °C (400 sccm H_2, 10 min), and annealed (400 sccm H_2, 30 min). Subsequently, graphene growth proceeded by introducing CH_4, and the tBLG domain was initiated by increasing the flow rates of H_2 (from 400 to 1000 sccm) and CH_4 (from 0.4 to 1 sccm). After 20 min of growth, the Cu foil was cooled by removing the sample away from the hot zone of the furnace.

Raman Spectroscopy Measurement. Micro-Raman spectra were obtained using a JY Horiba HR800 Raman spectrometer in the backscattering geometry. The wavelengths of excitation light are 532 nm (2.33 eV) and 633 nm (1.96 eV) in this work. The laser is focused on the tBLG through a 100× objective lens (numerical aperature (NA) = 0.9). And the laser power is kept below 0.5 mW to avoid damage to samples.

Density Functional Theory Calculation. The twisted bilayer graphene with twist angle of 13.2° was modeled to simulate the electronic and optical properties theoretically. The structural optimization is performed using the Quantum Espresso code,[16,17] with the LDA Troullier-Martins pseudopotential employed to describe electron−ion interactions and an origin-centered 6 × 6 × 1 k-point mesh distributed homogeneously in the first Brillouin zone. A vacuum layer of 20 Å along the z-direction is constructed to separate the system from its fictitious periodic images. Good convergence of residual stress and forces less than 1×10^{-2} kbar and 1×10^{-5} Ry/au, respectively, are obtained with a plane-wave energy cutoff of 120 Ry. The DOS is calculated non-consistently with a sufficiently denser 30 × 30 × 1 k-mesh on the base of ground-state charge density. Matrix elements of the momentum operator between valence and conduction bands have been achieved with the same k-point sampling as for DOS calculation to get the k-resolved electron−photon coupling strength under the dipole approximation. To calculate the phonon dispersion of AB-stacking double-layer graphene, the same pseudopotential and value of energy cutoff as for tBLG were used. The ground-state electron configuration is achieved sampled on a 24 × 24 × 1 k-point mesh centered on the origin, followed by the phonon dispersion calculation with 12 × 12 × 1 q-point mesh based on the density functional perturbation theory (DFPT).

https://doi.org/10.1021/acs.jpcc.2c03372
J. Phys. Chem. C 2022, 126, 10487−10493

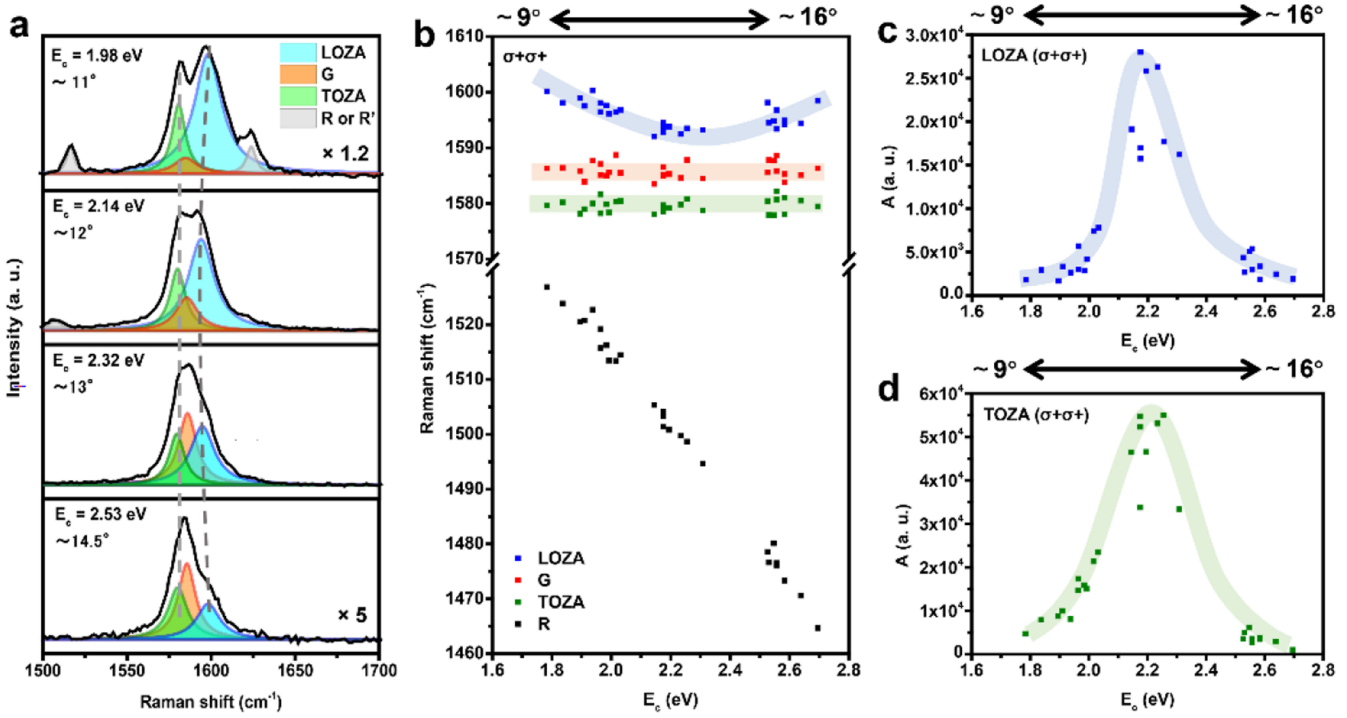

Figure 2. (a) Raman spectra of tBLG near the critical angle under (σ+σ+) configuration and 532 nm excitation with peak fitting. E_c is the optical transition band gap of each sample determined by optical contrast spectra. Dashed lines are guides to show frequency evolutions of two new Raman modes (LOZA & TOZA) with twist angle. (b) Frequency evolutions of LOZA, G, TOZA, and R modes as a function of twist angle. (c, d) Integrated intensity (A) evolutions of (c) LOZA and (d) TOZA modes as a function of twist angle. Thick curves in (b−d) are guides to show frequency and integrated intensity evolutions.

RESULTS AND DISCUSSION

Our tBLG were grown by CVD on Cu foil using a heterosite nucleation strategy and then transferred onto a SiO_2/Si substrate for all subsequent measurements.[15] Figure 1a shows optical images of CVD-grown Bernal-stacked BLG and tBLG with twist angles of ∼11°, 13°, and 15°, respectively. The sharp edges of the hexagonal tBLG domains can be used to roughly determine the twist angle, and the color in the bilayer region can assist the characterization of the twist angle (only for a twist angle between 10 and 15° in this work).[18] For example, the tBLG with a twist angle of ∼11°, 13°, and 15° present green, purple, and yellow colors were observed with optical microscopy. Furthermore, optical contrast spectra are used to characterize the twist angle precisely. Figure 1b shows the optical contrast spectra of 11°, 13°, and 15° tBLG in Figure 1a, which presents absorption peaks at ∼620, 550, and 450 nm, respectively, corresponding to the energies of optical transition band gaps between two VHS.[3,5]

The HRRS is obtained by exciting the sample using circularly polarized light and collecting the Raman scattered light with the same (σ+σ+) or opposite (σ+σ−) helicity as the incident light.[19,20] The experimental setup of HRRS is shown in Figure 1c. Left- or right-handed circularly polarized light is produced by a linear polarizer and the quarter-wave plate for incidence. And the scattered light with the same or opposite helicity is selected by setting the analyzer perpendicular or parallel to the incident polarizer. Figure 1d shows the HRRS of Bernal-stacked BLG and tBLG with twist angle of ∼11°, 13°, and 15° in Figure 1a, excited by a 532 nm laser. The G mode intensity of tBLG with a twist angle of ∼13° is much higher than that of a Bernal-stacked BLG due to the resonance enhancement between the VHS, which is consistent with previous reports.[4−6] For the G mode of 0° tBLG (Bernal-stacked tBLG), the helicity of Raman scattered light is opposite to that of the excitation light (Figure 1d), which can be understood by the Raman helicity selection rule or the conservation law of pseudoangular momentum.[21−23] For tBLG with twist angles of 11°, 13°, and 15°, the G peak under (σ+σ−) configuration can be perfectly fitted with a single Lorentz peak, but the peak shape under (σ+σ+) configuration is extremely unusual, especially for the 11° tBLG, which shows obvious peak splitting. We also measure the HRRS of twisted bilayer graphene with a twist angle of 16.5° (away from the critical angle of ∼13°), which shows similar results of 0° tBLG (Bernal-stacked tBLG, Figure S1). Besides, when the wavelength of the excitation laser is changed to 633 nm, the similar peak shape and splitting behavior near the critical angle (∼10°) can also be observed under (σ+σ+) configuration (Figure S2). The above results indicate that the abnormal peak shape under (σ+σ+) configuration only appears near the critical angle when the energy of the excitation light is close to the optical transition band gap between the VHS.

Figure 2a shows the Raman spectra of tBLG near the critical angle under (σ+σ+) configuration and 532 nm excitation with peak fitting. E_c is defined as the corresponding energy of peak position in the optical contrast spectra of tBLG, which is directly related to the twist angle.[3,18,24] It is worth noting that the G mode intensity is theoretically zero under (σ+σ+) configuration according to Raman helicity selection rules,[25] but in experiments the intensity can only be suppressed to a small yet nonzero value due to instrumental error such as the imperfect polarization configuration. This nonzero instrumental error is also observed in our HRRS experiment of silicon T_{2g} mode, which should have zero intensity under (σ+σ+)

https://doi.org/10.1021/acs.jpcc.2c03372
J. Phys. Chem. C 2022, 126, 10487−10493

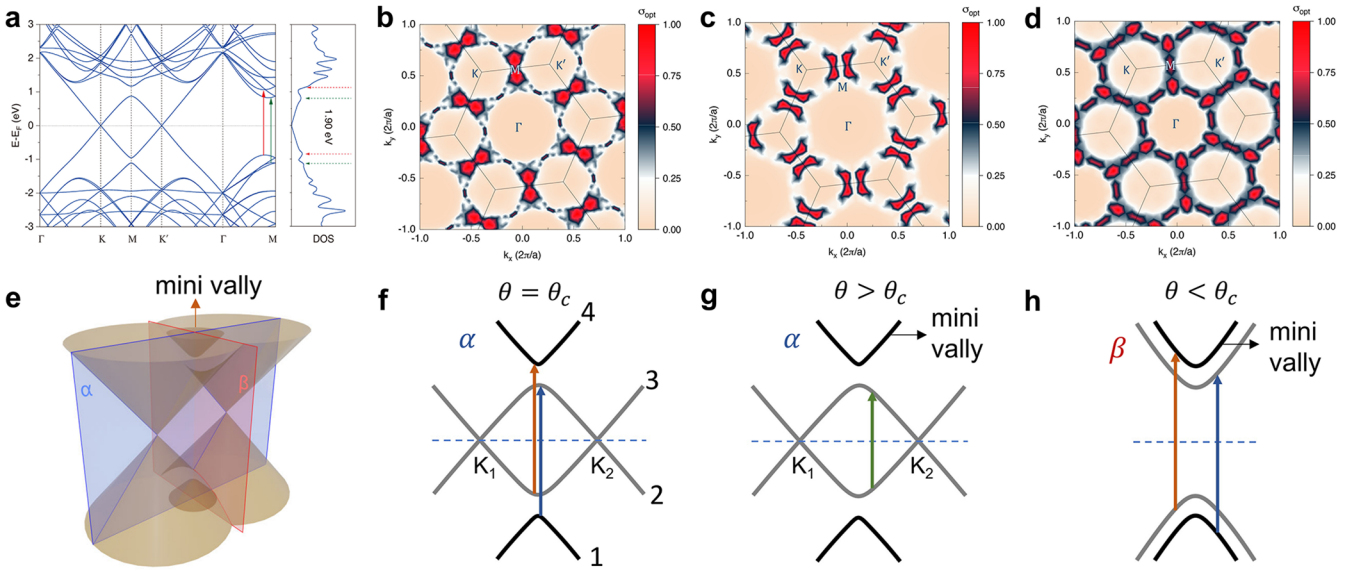

Figure 3. (a) Calculated band structure and DOS of 13.2° tBLG. Red and green arrows indicate two optically allowed electron transition pathways. (b–d) Electron–Photon coupling strength mapping in Brillouin zone with the excitation energy (b) equals (1.9 eV), (c) smaller (1.6 eV) or (d) larger (2.2 eV) than the optical transition band gap between VHS. (e) Corresponding three-dimensional low-energy band structure of tBLG near the M point. Red plane, α-plane; blue plane, β-plane. (f–h) Dominant electron–photon coupling pathways for situations when the photon energy is (f) equal ($\theta = \theta_c$), (g) small ($\theta < \theta_c$), or (h) larger ($\theta > \theta_c$) than the optical transition band gap between VHS. Dashed horizontal line indicates Fermi level at Dirac point.

configuration (Figure S3). Therefore, the nonzero G mode intensity error will also contribute to the abnormal peak shape under (σ+σ+) configuration and should be considered in the peak fitting. In fact, the nonzero G mode provides a perfect benchmark to fit the peak positions, since the G peak remains at the same frequencies for both (σ+σ+) and (σ+σ−) configurations. According to previous reports, the G band will split under stain,[26,27] but the splitting under (σ+σ+) configuration must not result from strain because the G mode shows a perfect single Lorentz peak under (σ+σ−) configuration, and thus the nonzero instrumental error of G mode should remain its single Lorentz peak feature with frequency of ∼1585 cm^{-1}. For 11° tBLG in Figure 2a, two intensity maximums of the split peak shape locate below and above the frequency of the G mode (Figure S4), meaning that there must be another two peaks contributing to the splitting. Considering all of the discussions above, the Raman spectra of tBLG near the critical angle under (σ+σ+) configuration are finally fitted with three single Lorentz peaks (Figure 2a): the G mode at 1585 cm^{-1} and the other two modes at the lower and higher frequencies than G mode, referred to as TOZA and LOZA modes, respectively. The assignment of TOZA and LOZA modes will be explained below.

To explore the peak frequency evolution with twist angle under (σ+σ+) configuration, we measure the HRRS of 30 tBLG samples with their twist angles ranging from 9° to 15°. Figure 2b shows the frequencies of LOZA, G, TOZA, and R modes as a function of E_c. The range of twist angles is labeled on the top of the figure for reference (Figure 2b–d). While the frequencies of TOZA and G modes stay constant with different twist angles, the LOZA mode blueshifts when the twist angle deviates from the critical angle. The frequency of the R mode redshifts with increased twist angles, which is consistent with previous reports and proves the accuracy of determining a twist angle using optical contrast spectra.[28] The integrated intensities (A) of the two new Raman modes as a function of twist angle are shown in Figure 2c,d. These two Raman modes display a similar enhancement behavior as that of the G mode (Figure S5), which can be explained by the mechanism of the VHS resonance.[4−6] HRRS for tBLG near the critical angle under 633 nm excitation is also investigated (Figures S6–S8), which shows the same trend of frequency and intensity evolution regardless of a different critical angle.

To further understand the origin of these two new Raman modes, we first analyze the electron–photon coupling of their Raman scattering process. Figure 3a is the band structure and DOS for tBLG with twist angle of 13.2° calculated by density functional theory (DFT). Figure 3b–d indicates the strength of electron–photon coupling at different locations in the Brillouin zone with the excitation energy equals (1.9 eV, Figure 3b), smaller (1.6 eV, Figure 3c) or larger (2.2 eV, Figure 3d) than the optical transition band gap between VHS. The calculation results indicate that the electron–photon coupling is mainly contributed from locations near the M point in the Brillouin zone when the laser energy equals the transition gap between VHS ($\theta = \theta_c$, Figure 3b), in the area along the M-K direction when the laser energy is smaller than the gap ($\theta > \theta_c$, Figure 3c) and in the area along M-Γ direction when the laser energy is larger than the gap ($\theta < \theta_c$, Figure 3d). The three-dimensional low-energy band structure of tBLG is presented in Figure 3e. We define the α-plane (blue plane) as the plane passing both axes of the Dirac cones, whereas the β-plane (red plane) is the bisector plane of the two Dirac cones. Figure 3f describes the electron transition near the M point when the photon energy equals the optical transition band gap of VHS. Noting that the optical transition band gap between VHS refers to the energy between bands 1 and 3 (or bands 2 and 4), because other electron transition from band 2 to band 3 (or from band 1 to band 4) is forbidden at the M point.[3,4,29] When the photon energy is less than the optical transition band gap between VHS ($\theta > \theta_c$, Figure 3g), the electron transition mainly occurs in the α-plane according to the calculation of

https://doi.org/10.1021/acs.jpcc.2c03372
J. Phys. Chem. C 2022, 126, 10487−10493

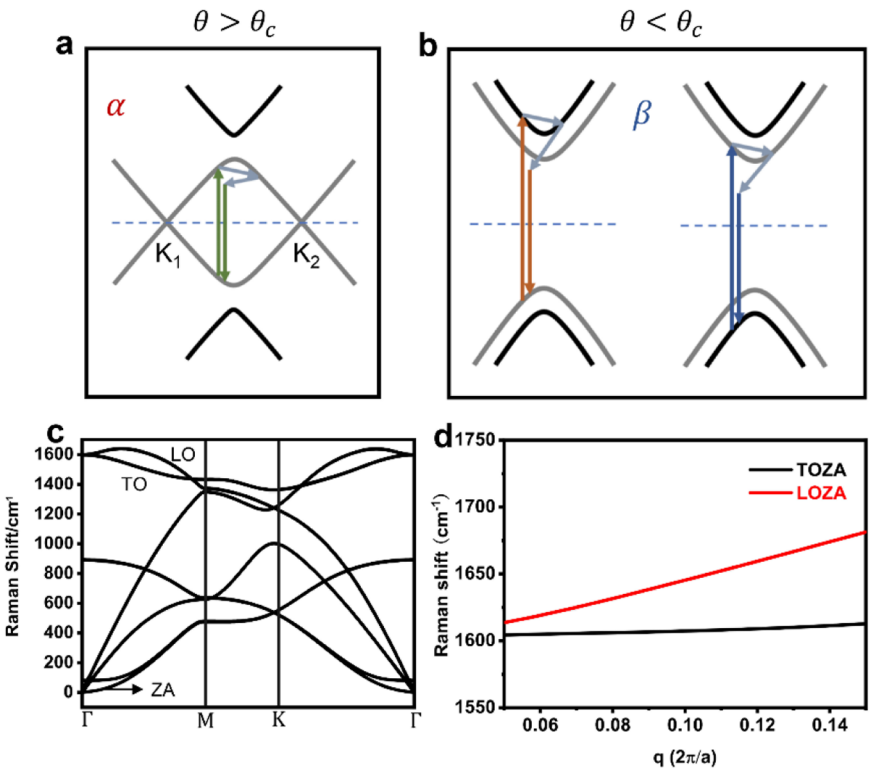

Figure 4. (a, b) Dominant Raman scattering pathways for situations of (a) $\theta > \theta_c$ and (b) $\theta < \theta_c$. Dashed horizontal line indicates Fermi level at Dirac point. (c) Calculated phonon dispersion curve for Bernal-stacked bilayer graphene. (d) Calculated frequency evolution of LOZA and TOZA modes as a function of phonon momentum near the Γ point. The "a" in the horizontal axis represents the lattice constant of graphene.

electron−photon coupling strength in the Brillouin zone (Figure 3c). However, when the photon energy is larger than the optical transition band gap between VHS ($\theta < \theta_c$, Figure 3h), the electron transition will mainly occur in the β-plane according to the calculation results in Figure 3d.

Now, we discuss the electron−phonon interaction in the Raman scattering process of the two newly observed modes. As the frequency of the LOZA mode varies obviously with photon energy and twist angle (Figure 2b and Figure S7a), it should be a second-order Raman scattering mode with Raman scattering pathway sensitive to the change of excitation energy and band structures.[30,31] Furthermore, we assume that the TOZA mode also results from a second-order Raman scattering process, because the twist angle dependence and resonance behaviors of the two modes are very alike and can be well-explained by a similar scattering model discussed below. Because the frequencies of two newly observed modes are very close to that of the the G mode, it is reasonable to assume that they are closely related to the LO and TO phonons near the center of the Brillouin zone. According to previous reports, new Raman modes observed in tBLG such as R and R′ modes are assisted by the inelastic scattering from a θ-dependent wavevector provided by the Moiré superlattice.[28,32] However, the new Raman modes observed in this work have a different frequency and twist angle dependence behavior from R and R′ modes, so they must have different scattering pathways to satisfy the requirement of the energy and momentum conservation. Moreover, the LO or TO phonon involved in the scattering of these two Raman modes must have a relatively small momentum **q** because their frequencies are very close to the G mode whose momentum is zero.[30,31] Considering all of the requirements above, we finally assigned the new phonon modes as a second-order Raman scattering combination mode of LO+ZA and TO+ZA with an intra-mini valley scattering pathway near the low-energy saddle points.

Figure 4a,b shows the schematic diagrams of the new phonon scattering pathways when the photon energy is smaller ($\theta > \theta_c$, Figure 4a) or larger ($\theta < \theta_c$, Figure 4b) than the optical transition band gap between VHS. The LOZA and TOZA modes share the same electron−photon coupling process as the G mode near the M point, which explains their similar resonance enhancement behavior (Figure 2c,d and Figure S7b,c). Although LOZA and TOZA modes are second-order Raman scattering, the momentum of phonons associated in the scattering process is very small. When the photon energy is smaller than the optical transition band gap between VHS, phonon scattering pathways of LOZA and TOZA modes in the α-plane can be seen from Figure 4a. With decreased photon energy, the electron will be excited further away from the M point, which leads to increased phonon momentum in order to satisfy momentum conservation in an electron−phonon interaction. Figure 4b shows the scattering pathway in the β-plane when the photon energy is larger than the optical transition band gap between VHS. In this case, the increase of photon energy will also result in the shift of excitation location away from the M point with a larger phonon momentum. In short, the momentum of the phonon is minimal at $\theta = \theta_c$ and increases when the laser energy deviates from the optical transition band gap between VHS. Then we calculate the phonon dispersion curve to investigate the frequency changes of LOZA and TOZA modes with different phonon momentum (Figure 4c,d). While the dispersion curves shown were calculated for Bernal-stacked BLG, they are expected to be similar for tBLG for the relevant modes studied here. The

https://doi.org/10.1021/acs.jpcc.2c03372
J. Phys. Chem. C 2022, 126, 10487−10493

frequency of the LOZA mode increases with the increase of phonon momentum, while the frequency of the TOZA mode almost remains unchanged as the momentum changes. Therefore, the frequency of the LOZA mode will increase when the twist angle deviates from the critical angle, and the frequency of the TOZA mode should remained unchanged. This result is in good agreement with our experimental observation in Figure 2b and Figure S7a, which further verifies the existence of the intra-mini valley scattering pathways. It is worth noticing that, although the phonon momentum seems to be zero when $\theta = \theta_c$ according to our analysis in Figure 4a,b, the real phonon momentum must be larger than zero in this situation because the electron−photon coupling is not perfectly at the M point even at the resonance condition as shown in Figure 3a. Therefore, the frequencies of LOZA and TOZA modes will not be equal to the G mode even at critical twist angle. In a word, the analysis of the frequency and the intensity confirm the assignment of the LO+ZA and TO+ZA as well as an intra-mini valley scattering pathway near the low-energy saddle points.

CONCLUSION

In summary, two Raman active modes near G modes are observed in tBLG for the first time using HRRS, which demonstrates the existence of the intra-mini valley phonon scattering pathway near the low-energy saddle points. These two new modes, which are assigned as TOZA and LOZA combination modes, can only be revealed under $\sigma+\sigma+$ configuration of HRRS under which G mode intensity is suppressed. The intensities of these two modes display a concomitant resonance enhancement with G mode near the critical angle, indicating that they also have a VHS resonance mechanism. The measured LOZA frequency increases with twist angle deviating from the critical angle, while the TOZA frequency almost remains unchanged. Combining the above experimental results with the band structure and electron−photon coupling analysis, the new phonon scattering pathways are confirmed as the intra-mini valley scattering process, and the twist angle dependence behavior is explained by phonon dispersion calculations. These results provide a deeper understanding about the detailed band structure near the saddle points and offer an insight into the VHS-related physics from the view of electron−phonon interactions.

ASSOCIATED CONTENT

Supporting Information

The Supporting Information is available free of charge at https://pubs.acs.org/doi/10.1021/acs.jpcc.2c03372.

HRRS of tBLG with twist angles of ∼16.5° and 0° with 532 nm excitation; HRRS of tBLG near critical angle with 633 nm excitation; HRRS of silicon T_{2g} mode; normalized HRRS of tBLG with twist angles of ∼11° and 12°; integrated intensity evolution of G mode as a function of twist angle under ($\sigma+\sigma+$) configurations with 532 nm excitation; Raman spectra of tBLG near critical angle under ($\sigma+\sigma+$) configuration and 633 nm excitation with peak fitting; frequency evolutions (LOZA, G, TOZA, and R modes) and integrated intensity (LOZA, TOZA, and G modes) as a function of twist angle under ($\sigma+\sigma+$) configuration and 633 nm excitation (PDF)

AUTHOR INFORMATION

Corresponding Author

Lianming Tong − *Center for Nanochemistry, Beijing Science and Engineering Center for Nanocarbons, Beijing National Laboratory for Molecular Sciences, College of Chemistry and Molecular Engineering, Peking University, Beijing 100871, P. R. China;* orcid.org/0000-0001-7771-4077; Email: tonglm@pku.edu.cn

Authors

Bo Xu − *Academy for Advanced Interdisciplinary Studies, Peking University, Beijing 100871, P. R. China; Center for Nanochemistry, Beijing Science and Engineering Center for Nanocarbons, Beijing National Laboratory for Molecular Sciences, College of Chemistry and Molecular Engineering, Peking University, Beijing 100871, P. R. China*

He Hao − *Center for Nanochemistry, Beijing Science and Engineering Center for Nanocarbons, Beijing National Laboratory for Molecular Sciences, College of Chemistry and Molecular Engineering, Peking University, Beijing 100871, P. R. China*

Jianqi Huang − *Shenyang National Laboratory for Materials Science, Institute of Metal Research, Chinese Academy of Sciences, Shenyang 110016, P. R. China*

Yan Zhao − *Academy for Advanced Interdisciplinary Studies, Peking University, Beijing 100871, P. R. China; Center for Nanochemistry, Beijing Science and Engineering Center for Nanocarbons, Beijing National Laboratory for Molecular Sciences, College of Chemistry and Molecular Engineering, Peking University, Beijing 100871, P. R. China*

Teng Yang − *Shenyang National Laboratory for Materials Science, Institute of Metal Research, Chinese Academy of Sciences, Shenyang 110016, P. R. China*

Jin Zhang − *Center for Nanochemistry, Beijing Science and Engineering Center for Nanocarbons, Beijing National Laboratory for Molecular Sciences, College of Chemistry and Molecular Engineering, Peking University, Beijing 100871, P. R. China;* orcid.org/0000-0003-3731-8859

Complete contact information is available at: https://pubs.acs.org/10.1021/acs.jpcc.2c03372

Author Contributions

‖B.X. and H.H. contributed equally to the work. B.X. and H.H. conceived the idea and designed the experiments. J.H. and T.Y. performed the theoretical calculations. B.X., H.H., and L.T. wrote the manuscript. The work was supervised by L.T. and J.Z. All of the authors discussed the results and commented on the manuscript.

Notes

The authors declare no competing financial interest.

ACKNOWLEDGMENTS

The authors thank Beijing Graphene Institute for providing tBLG samples. This work was financially supported by the Ministry of Science and Technology of China (Grant Nos. 2018YFA0703502, 2016YFA0200104, and 2017YFA0206301), the National Natural Science Foundation of China (Grant Nos. 52021006, 51720105003, 21790052, 21974004, and 52031014), the Strategic Priority Research Program of CAS (XDB36030100), and the Beijing National Laboratory for Molecular Sciences (BNLMS-CXTD-202001).

REFERENCES

(1) Vanhove, L. The occurrence of singularities in the elastic frequency distribution of a crystal. *Phys. Rev.* **1953**, *89*, 1189−1193.
(2) Kim, C. J.; Sanchez-Castillo, A.; Ziegler, Z.; Ogawa, Y.; Noguez, C.; Park, J. Chiral atomically thin films. *Nat. Nanotechnol.* **2016**, *11*, 520−524.
(3) Havener, R. W.; Liang, Y.; Brown, L.; Yang, L.; Park, J. Van Hove singularities and excitonic effects in the optical conductivity of twisted bilayer graphene. *Nano Lett.* **2014**, *14*, 3353−3357.
(4) Havener, R. W.; Zhuang, H.; Brown, L.; Hennig, R. G.; Park, J. Angle-resolved Raman imaging of inter layer rotations and interactions in twisted bilayer graphene. *Nano Lett.* **2012**, *12*, 3162−3167.
(5) Kim, K.; Coh, S.; Tan, L. Z.; Regan, W.; Yuk, J. M.; Chatterjee, E.; Crommie, M. F.; Cohen, M. L.; Louie, S. G.; Zettl, A. Raman spectroscopy study of rotated double-layer graphene: misorientation-angle dependence of electronic structure. *Phys. Rev. Lett.* **2012**, *108*, 246103.
(6) He, R.; Chung, T.-F.; Delaney, C.; Keiser, C.; Jauregui, L. A.; Shand, P. M.; Chancey, C. C.; Wang, Y.; Bao, J.; Chen, Y. P. Observation of low energy Raman modes in twisted bilayer graphene. *Nano Lett.* **2013**, *13*, 3594−3601.
(7) Li, G.; Luican, A.; Lopes dos Santos, J. M. B.; Castro Neto, A. H.; Reina, A.; Kong, J.; Andrei, E. Y. Observation of Van Hove singularities in twisted graphene layers. *Nat. Phys.* **2010**, *6*, 109−113.
(8) Yuan, N. F. Q.; Isobe, H.; Fu, L. Magic of high-order van Hove singularity. *Nat. Commun.* **2019**, *10*, 5769.
(9) Castro Neto, A. H.; Guinea, F.; Peres, N. M. R.; Novoselov, K. S.; Geim, A. K. The electronic properties of graphene. *Rev. Mod. Phys.* **2009**, *81*, 109−162.
(10) Reich, S.; Maultzsch, J.; Thomsen, C.; Ordejon, P. Tight-binding description of graphene. *Phys. Rev. B* **2002**, *66*, No. 035412.
(11) Grueneis, A.; Attaccalite, C.; Wirtz, L.; Shiozawa, H.; Saito, R.; Pichler, T.; Rubio, A. Tight-binding description of the quasiparticle dispersion of graphite and few-layer graphene. *Phys. Rev. B* **2008**, *78*, 205425.
(12) Bistritzer, R.; MacDonald, A. H. Moire bands in twisted double-layer graphene. *Proc. Natl. Acad. Sci. U.S.A.* **2011**, *108*, 12233−12237.
(13) Lopes dos Santos, J. M. B.; Peres, N. M. R.; Castro Neto, A. H. Graphene bilayer with a twist: Electronic structure. *Phys. Rev. Lett.* **2007**, *99*, 256802.
(14) Malard, L. M.; Pimenta, M. A.; Dresselhaus, G.; Dresselhaus, M. S. Raman spectroscopy in graphene. *Phys. Rep.* **2009**, *473*, 51−87.
(15) Sun, L.; Wang, Z.; Wang, Y.; Zhao, L.; Li, Y.; Chen, B.; Huang, S.; Zhang, S.; Wang, W.; Pei, D.; et al. Hetero-site nucleation for growing twisted bilayer graphene with a wide range of twist angles. *Nat. Commun.* **2021**, *12*, 2391.
(16) Giannozzi, P.; Baroni, S.; Bonini, N.; Calandra, M.; Car, R.; Cavazzoni, C.; Ceresoli, D.; Chiarotti, G. L.; Cococcioni, M.; Dabo, I.; et al. QUANTUM ESPRESSO: a modular and open-source software project for quantum simulations of materials. *J. Phys.: Condens. Matter* **2009**, *21*, 395502.
(17) Giannozzi, P.; Andreussi, O.; Brumme, T.; Bunau, O.; Nardelli, M. B.; Calandra, M.; Car, R.; Cavazzoni, C.; Ceresoli, D.; Cococcioni, M.; et al. Advanced capabilities for materials modelling with QUANTUM ESPRESSO. *J. Phys.: Condens. Matter* **2017**, *29*, 465901.
(18) Campos-Delgado, J.; Algara-Siller, G.; Santos, C. N.; Kaiser, U.; Raskin, J. P. Twisted bi-layer graphene: microscopic rainbows. *Small* **2013**, *9*, 3247−3251.
(19) Xu, B.; Xu, S.; Zhao, Y.; Zhang, S.; Feng, R.; Zhang, J.; Tong, L. Determining the oblique angle of vertical graphene arrays using helicity-resolved Raman spectroscopy. *J. Phys. Chem. C* **2021**, *125*, 8353−8359.
(20) Zhao, Y.; Zhang, S.; Shi, Y.; Zhang, Y.; Saito, R.; Zhang, J.; Tong, L. Characterization of excitonic nature in Raman spectra using circularly polarized light. *ACS Nano* **2020**, *14*, 10527−10535.
(21) Tatsumi, Y.; Kaneko, T.; Saito, R. Conservation law of angular momentum in helicity-dependent Raman and Rayleigh scattering. *Phys. Rev. B* **2018**, *97*, 195444.
(22) Chen, C.; Chen, X.; Deng, B.; Watanabe, K.; Taniguchi, T.; Huang, S.; Xia, F. Probing interlayer interaction via chiral phonons in layered honeycomb materials. *Phys. Rev. B* **2021**, *103*, No. 035405.
(23) Loudon, R. The Raman effect in crystals. *Adv. Phys.* **2001**, *50*, 813−864.
(24) Cheon, Y.; Kim, Y.; Park, M.; Oh, J.; Koo, E.; Sim, E.; Ju, S.-Y. Excited state charge transfer promoted Raman enhancement of copper phthalocyanine by twisted bilayer graphenes. *Carbon* **2022**, *188*, 305−314.
(25) Zhao, Y.; Xu, B.; Tong, L.; Zhang, J. The helicity of Raman scattered light: principles and applications in two-dimensional materials. *Sci. China Chem.* **2022**, *65*, 269−283.
(26) Mohiuddin, T. M. G.; Lombardo, A.; Nair, R. R.; Bonetti, A.; Savini, G.; Jalil, R.; Bonini, N.; Basko, D. M.; Galiotis, C.; Marzari, N.; et al. Uniaxial strain in graphene by Raman spectroscopy: G peak splitting, Gruneisen parameters, and sample orientation. *Phys. Rev. B* **2009**, *79*, 205433.
(27) Xu, B.; Mao, N.; Zhao, Y.; Tong, L.; Zhang, J. Polarized Raman spectroscopy for determining crystallographic orientation of low-dimensional materials. *J. Phys. Chem. Lett.* **2021**, *12*, 7442−7452.
(28) Eliel, G. S. N.; Moutinho, M. V. O.; Gadelha, A. C.; Righi, A.; Campos, L. C.; Ribeiro, H. B.; Chiu, P.-W.; Watanabe, K.; Taniguchi, T.; Puech, P.; et al. Intralayer and interlayer electron-phonon interactions in twisted graphene heterostructures. *Nat. Commun.* **2018**, *9*, 1221.
(29) Moon, P.; Koshino, M. Optical absorption in twisted bilayer graphene. *Phys. Rev. B* **2013**, *87*, 205404.
(30) Wu, J.; Lin, M.; Cong, X.; Liu, H.; Tan, P. Raman spectroscopy of graphene-based materials and its applications in related devices. *Chem. Soc. Rev.* **2018**, *47*, 1822−1873.
(31) Zhang, S.; Zhang, N.; Zhao, Y.; Cheng, T.; Li, X.; Feng, R.; Xu, H.; Liu, Z.; Zhang, J.; Tong, L. Spotting the differences in two-dimensional materials - the Raman scattering perspective. *Chem. Soc. Rev.* **2018**, *47*, 3217−3240.
(32) Carozo, V.; Almeida, C. M.; Ferreira, E. H. M.; Cancado, L. G.; Achete, C. A.; Jorio, A. Raman signature of graphene superlattices. *Nano Lett.* **2011**, *11*, 4527−4534.

https://doi.org/10.1021/acs.jpcc.2c03372
J. Phys. Chem. C 2022, 126, 10487−10493